Journal of Nuclear Materials 407 (2010) 71–77

Contents lists available at ScienceDirect

Journal of Nuclear Materials

journal homepage: www.elsevier.com/locate/jnucmat

HTR Fuel Waste Management: TRISO separation and acid-graphite intercalation compounds preparation

Fabrice Guittonneau, Abdesselam Abdelouas *, Bernd Grambow

SUBATECH, UMR 6457, IN2P3/CNRS-Ecole des Mines de Nantes/Université de Nantes, 4 Rue Alfred Kastler, 44307 Nantes Cedex 3, France

ARTICLE INFO

Article history:
Received 4 May 2010
Accepted 14 September 2010

ABSTRACT

Considering the need to reduce waste production and greenhouse emissions and still keeping high energy efficiency, various 4th generation nuclear energy systems have been proposed. As far as graphite-moderated reactors are concerned (future high temperature fast or thermal reactors), one of the key issues is the large volumes of irradiated graphite encountered. With the objective to reduce volume of waste in the HTR concept, it is very important to be able to separate the fuel from low level activity graphite representing a large volume. The separated TRISO particles can then be reprocessed for waste separation or disposed off in geological repository. In addition, preparation of acid-GICs from the separated graphite may constitute a way to recycle this waste.

We used HTR-type compact fuel with ZrO_2 TRISO particles to test two separation methods: low ($H_2SO_4 + H_2O_2$) and high ($H_2SO_4 + HNO_3$) temperature acid treatments. In both cases the TRISO separation was complete but some TRISO layers oxidized at high temperature. At low temperature, the desegregation of graphite grains is facilitated by intercalation of sulfuric acid between the graphene layers. The acid-GIC obtained consists of pure phases of high quality suggesting their potential industrial recycling.

1. Introduction

With the increase of energy demand and the international wish to preserve the environment, nuclear energy may help to achieve these goals. One of the main objectives of nuclear industry is to reduce the waste volumes (waste fuel + decommissioning products). Operation of graphite-moderated reactors such as French UNGG (uranium naturel graphite gaz), English AGR (advanced gas reactor) and Russian RBMK (high power channel-type reactor) produced large quantities of contaminated graphite that need to be recycled or disposed off in deep geological formations. Thereby, in June 2006, a French law (No. 2006-739) requests to provide a selection of a disposal facility for the irradiated graphite from the UNGG reactors for 2013.

Future reactors technologies including HTR (high temperature reactor) will use graphite blocks for reflector and fuel. Compacts from block-type and pebbles from PBMR (pebble bed modular reactor) will need reprocessing to separate the highly radioactive TRISO particles from the low level irradiated graphite. Some previous studies summarized in [1] dealt with graphite management such as furnace incineration, fluidized bed incineration, laser incineration, encapsulation into matrices (cement, bitumen, polymers, glass...), but economical and environmental criterions are not really satisfied, allowing to treat even a small fraction of the about 250,000 tonnes of irradiated graphite which has been accumulated worldwide. A few studies on TRISO separation from graphite have been conducted [2,3] and showed some weaknesses like high cost, coating failure, partial separation, complexity...The separated TRISO could be vitrified and disposed off in deep geological formation as suggested by Abdelouas et al. [4]. However, heat load must be taken into consideration to determine whether TRISO separation provides volume reduction advantages for geological disposal. Reprocessing of the irradiated TRISO could also be considered for U and Pu recovery and waste separation.

We present in this paper a fast method with potential economical advantages, which allows a total desegregation of graphite blocks, still preserving the integrity of TRISO particles. The method consists of intercalating compounds into graphite layers to cause grain separation.

Since graphite intercalation compounds (GICs) were discovered by Schffäutl by intercalation of potassium, a great number of GICs were synthesized with intercalates such as alkali, earth alkali, transition metal chlorides, acids, halogens, etc., in gas–solid or liquid–solid phase. A good summary of synthesis types can be found in the book of Enoki et al. [5]. These authors give a definition of the stage number n which "is defined as the structure in which intercalates are accommodated regularly in every nth graphitic gallery". We studied in this paper the desegregation of graphite via the intercalation of H_2SO_4. In acid treatment, graphite is partially oxidized. Acids play the role of electron acceptor from graphite π-bonds.

* Corresponding author. Tel.: +33 251858462; fax: +33 251858452.
E-mail address: abdesselam.abdelouas@subatech.in2p3.fr (A. Abdelouas).

0022-3115/$ - see front matter © 2010 Published by Elsevier B.V.
doi:10.1016/j.jnucmat.2010.09.026

Reactions with acids are possible by oxidant-assisted (HNO_3, CrO_3, $KMnO_4$, $HClO_4$, H_2O_2...) intercalation or by electrochemical intercalation. Usually, high stage intercalation via oxidant-assisted intercalation is harder to obtain than via electrochemical process. Many studies worked on sulfuric acid intercalation [6–12] and sulfur-free acid intercalation [13–18]. Acid-GICs are often used as intermediate products before starting the exfoliation process, during which, above a critical temperature, a large thermal expansion by as much as a factor of 300 occurs, leading to products with high surface areas (up to 85 m^2/g). The exfoliation occurs when the gas pressure exceeds the internal stress parallel to the *c*-axis. The exfoliated graphite (EG) often has the shape of the famous "worm structure", depending of the raw material properties and the GIC preparation. Compressed-EGs (CEGs) are industrially manufactured by Toyo Tanso notably, for the fabrication of flexible graphite sheets, gaskets, furnace insulators... [19] or simply non-compressed EG for oil sorption [20–26]. An excellent review on CEGs can be found in the publication of Celzard et al. [27]. CEGs are of great interest because nuclear graphite can be transformed in CEG for "second life" applications. However, the recycling of the graphite could be limited due to the remaining radioactivity of the treated material.

2. Materials and methods

Raw materials are 'compacts' manufactured by AREVA NP from natural graphite. Their manufacture is explained in reference [28]. To summarize it, graphite powder is mixed with a phenolic resin and then TRISO particles are added. Green compact is formed by a double piston and thermal treatment is made under vacuum at 1800 °C. Compacts' length is about 47.8 mm and the mean diameter about 12.4 mm (Fig. 1). We can notice here that phenolic resin does not graphitize during thermal treatment and forms an amorphous carbon, which has poor mechanical properties and reacts more easily than "real" graphite. XRD analysis of the graphite's compact gave lattice parameters as follow: $a = 2.4645$ Å and $c = 6.7171$ Å. These parameters are little larger than for usual graphite. Crystallite size calculations via the method of Scherrer showed $L_a = (412 \pm 18)$ Å and $L_c = (360 \pm 51)$ Å, but this method is very sensitive to defects into crystals, e.g. dislocation, vacancy, etc. These distances correspond to the sizes of 'perfect crystals'. SEM (scanning electron microscope) and TEM (transmission electron microscope) observations indicated very much larger crystals, up to micrometer scale in the direction of *a*.

The compacts contain fuel spheres, the TRISO particles. For our experiments, for radiation protection purposes the TRISO particles kernels were made of ZrO_2 instead of UO_2. They consist of 530 μm diameter kernels surrounded by four protective layers insuring chemical and mechanical integrities. These four layers are from the center to the outside porous pyrolytic carbon (buffer of 90 μm thickness), dense inner pyrolytic carbon (iPyC of 40 μm), silicon carbide (SiC of 35 μm) and a final outer pyrolytic carbon (oPyC of 40 μm). Fabrication, scheme and physical properties of fuel particles are described in [3,29–34]. The pyrolytic carbon is very pure graphite analog and reacts very slowly. Each compact containing 20% volume packing fraction comprises about 3000 TRISO particles.

Two types of experiences were conducted: high pressure/high temperature microwave treatments (MW) and room temperature chemical treatments under air atmosphere (RT).

2.1. Preparation of GICs via microwave

For MW treatments, an Anton Paar Multiwave 3000 mineralization device was used to separate graphite from the TRISO particles. Because of the limited capacity of this device, compacts (containing 10% packing fraction, PF) were cut in disks or half-disks of about 3 mm height. Samples were placed into the Teflon vessels with 10 mL of a mixture of sulfuric acid (95%) and nitric acid (69%). The reaction between these two acids is well known and creates the nitronium ion which is very oxidant:

$$HNO_3 + H_2SO_4 \leftrightarrow H_2NO_3^+ + HSO_4^- \quad (1)$$

$$H_2NO_3^+ \leftrightarrow H_2O + NO_2^+ \quad (2)$$

Four vessels were simultaneously in operation. All sample masses and volumes and reagent acids are mentioned in Table 1 together with treatments results. Electric power, temperature, pressure and plateau were fixed in all experiments at 1400 W (constant rate at 140 W/min), 200 °C, 55 bar (limited at 0.5 bar/s) and 15 min, respectively. After cooling into the microwave oven, the resulting samples of intercalated graphite + TRISO particles were rinsed in ultra-pure water. Samples were centrifuged to separate the particles. GICs are dried into an air oven at 85 °C.

Solids (GICs) have been characterized by nitrogen adsorption at 77 K using the BET equation to estimate the specific surface area. The device employed was a Micromeritics ASAP 2010. X-ray diffraction analyses were conducted in a Siemens D5000 diffractometer using a Cu anode at $\lambda = 1.5406$ Å, $V = 40$ kV and $I = 30$ mA. Infrared measurements (Shimadzu FTIR device) were recorded from 400 cm^{-1} to 4000 cm^{-1} (resolution 4 cm^{-1}, 50 scans) and from 400 cm^{-1} to 1400 cm^{-1} (resolution 1 cm^{-1}, 50 scans), using KBr pellets of about 300 mg.

A part of each sample has been kept to proceed with the exfoliation process. These samples were placed into an alumina crucible and were rapidly heated at 1000 °C during 1 min in air. The intercalated sulfuric acid decomposed into SO_2, O_2 and H_2O. The exfoliated graphite (EG) did not have enough time to burn in CO_x: EG are known to be resistant versus heat and oxidation. The mass loss was monitored and BET measurement allows observing the increase of the surface during the transformation of GIC into EG.

Optical observations were conducted with a binocular microscope Leica MZ16 coupled with the software Leica Application Suite for the image capture. SEM characterizations were conducted with a JEOL 5800LV and image capture was made with the

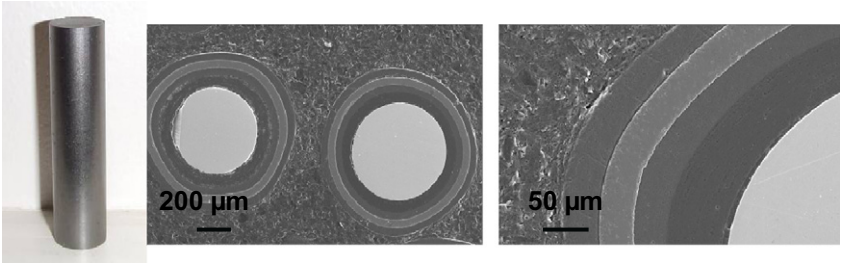

Fig. 1. Graphite compact (left) in which TRISO particles (center, right) are embedding.

Table 1
Details of samples characteristics for microwave treatments, and BET results.

# Sample	Initial mass (g)	Volume H_2SO_4 (mL)	Volume HNO_3 (mL)	Mass after washing and drying (g)	Mass increase (%)	BET after washing (m^2/g)	Heat treatment temperature (°C)	Average mass loss (%)	BET after heat treatment (m^2/g)	BET ratio
S10	0.245	10	0	0.300 disk swelling	22	NA	1000	−24	NA	–
S9N1	0.516	9	1	0.732	42	0.91		−48	3.47	3.83
S8N2	0.565	8	2	0.946	67	NA		−59	NA	–
S7N3	0.484	7	3	0.714	47	1.12		−52	4.39	3.91
S6N4	0.466	6	4	0.700	50	N.A.		−49	NA	–
S5N5	0.466	5	5	0.903	94	0.91		−61	2.27	2.48
N10	0.212	0	10	No separation	–	–	–	–	–	–

NA: not available.

Table 2
Preparation of H_2SO_4-graphite intercalation compounds (GICs) at room temperature and some of their properties.

# Sample	Initial mass (g)	Volume H_2O_2 (mL)	Volume H_2SO_4 (mL)	Approximate expansion volume variation (%)	Stage *n*	Heat treatment temperature (°C)	Average mass loss (%)	BET after heat treatment (m^2/g)
S20H1	10.581	1	20	500	2	1000	−56.3	36.1
S20H2	10.376	2		900	Not defined		−66.6	32.2
S20H3	10.583	3		1300	4		−57.5	29.0
S20H4	10.512	4		1600	3		−53.8	34.0

software SEMafore. The transmission electronic microscope was a HITACHI H-9000 NAR, operating at 300 kV, coupled with the software DigitalMicrograph™ for the image capture.

2.2. Preparation of high stages GICs at room temperature

Entire compacts (containing 20% PF) were used for this set of experiments. This method was used by Kang et al. [6] but we worked with different volume ratios and reagent concentrations. The first step of this treatment is the graphite oxidation by adding some hydrogen peroxide (1–4 mL per sample). We used H_2O_2 at 50% from Aldrich. Then, in a second step, we added sulfuric acid at 95% for the intercalation process. Table 2 details masses and volumes for each reagent. After less than one hour, the reaction was finished. New materials have the aspect of doughy black slurry. The reaction is expressed as:

$$H_2O_2 \rightarrow H_2O + O \quad (3)$$

$$24n\ C + mH_2SO_4 + 1/2O \rightarrow C_{24n}{}^{+}(HSO_4)^{-}(m-1)H_2SO_4 + 1/2H_2O \quad (4)$$

where n is the stage number and m is a stoichiometric coefficient. GICs were characterized by XRD to get information on the new crystallographic system. To avoid a possible de-intercalation, samples were not rinsed as previously with MW treatments but were analyzed as acid slurry and as soon as possible using the same material described in the previous paragraph. During X-ray diffraction analyses, a slackening of liquid was observed, probably H_2SO_4 and H_2O. X-ray diffraction allowed determining the sandwich thickness d_s defined by the distance between two graphene layers in which an intercalated compound is inserted. The new c parameter, called I_c, is linked to d_s, stage number n and initial c (6.717 Å) parameters by the relation:

$$I_c = d_s + 1/2c(n-1) \quad (5)$$

After XRD analyses, we proceeded with the exfoliation process in the same manner as previously. Specific surface area of EG was measured by the BET method (Table 2).

3. Results and discussion

3.1. MW treatments

3.1.1. Infrared, XRD and BET studies

All samples were analyzed after washing and drying. Analyses of samples by XRD were first conducted but diffractograms revealed mostly the graphite structure and no high stage GIC (n small) was found. Diffractograms present a low intensity and for samples S6N4 and S5N5, 0 0 2 and 0 0 4 peaks of graphite are visible with a little shoulder on the left of the 0 0 2 peaks. Samples S9N1 and S8N2 have these two peaks but shoulders become wide centered at angles 26.161° and 26.070°, respectively. These wide peaks indicate a decrease of coherence length of crystals and these two angles correspond to stages 21 and 16 for peaks 0 0 22 and 0 0 17, respectively (the peak 0 0 $n+1$ is always the strongest in H_2SO_4-GICs). The very low acid intercalation observed by XRD can therefore be explained by a de-intercalation of the acid during the washing with pure water. That is the reason why samples in the next set of experiments have not been washed.

Even though samples contain small amounts of acid, infrared spectra (Fig. 2) show several bands in the weak energy range for samples S*x*N*y* ($x \neq 0$). Natural graphite, samples N10 and EG do not have these absorption bands, presuming that these bands still indicate the presence of sulfur oxide in samples S*x*N*y* ($x \neq 0$), despite of washing. So, H_2SO_4 is present at a very low stage, not clearly defined. Regarding sample S10, intercalation of sulfuric acid is also possible without nitric acid. From reference [11], absorptions at energies 1010 and 1070 cm^{-1} can be assigned to the S=O bond but these authors worked with the SO_2 gas. The very intense peak at 1181 cm^{-1} can be assigned to the covalent sulfate group while peaks for the ionic sulfate are between 1070 and 1130 cm^{-1} (bonds in ionic sulfate are weaker than in covalent sulfate). So, the intense peak at 1181 cm^{-1} is indicative for the bonding of sulfate between two graphene layers by bonds C_g—O—(SO_2)—O—C_g, where C_g is a carbon from graphene. From reference [35], peaks at 576, 584, 593 and 615 cm^{-1} are also assigned to the covalent sulfate. The wide peak around 3440 cm^{-1} is attributed to the O—H bond. This peak being weaker for graphite, N10 and EG, we can suggest that the O-H signal comes from adsorbed

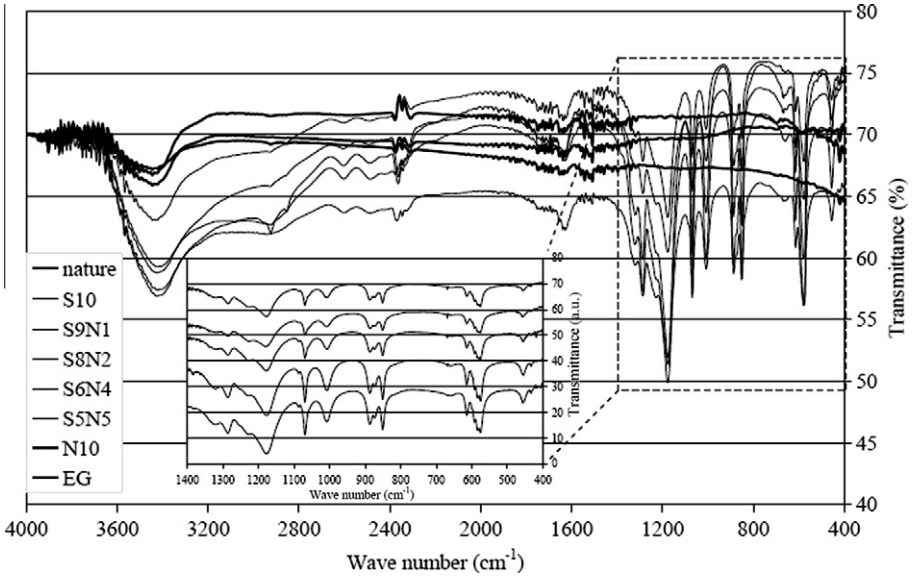

Fig. 2. Infrared spectra of rinsed H_2SO_4-graphite intercalation compounds (GICs) prepared by microwave, compared with natural graphite and exfoliated graphite. In medallion is represented a zoom of the "digital prints" region 400–1400 cm^{-1} where appear sulfur bands.

water (H_2SO_4-GICs are hygroscopic) or comes from H_2SO_4 or HSO_4^- respectively free or linked by bonds C_g—O—(SO_2)—OH.

The exfoliation process followed by the BET analyses indicates as well the presence of H_2SO_4 at low stage, since the surface area observed (<5 m^2/g) is small compared to EGs issued from high stage GICs, as mentioned in the reference [36]. Specific surface area ratios are then also weak (Table 1).

3.1.2. Microscopic characterizations of GIC, EG and TRISO particles

The main objective of this study being the separation of TRISO particles from the graphite matrix without breaking them, we had to preserve the integrity of the first accessible barrier of TRISO, i.e. oPyC. Hereafter are presented some optical and electronic microscopy photographs of some samples S*x*N*y* before and after exfoliation process, as well as of separated TRISO particles.

As shown in Fig. 3, sample S10 (without TRISO particles) swelled but the graphite grain crumbling did not occur, which does not allow for TRISO particles separation from the graphite matrix. But this swelling is still accompanied by an acid intercalation, proved during the exfoliation process, showing large size worms-like structures (150 μm diameter and more than 1 mm length) and graphene layers moved away from each other. The graphite desegregation required application of a mixture of nitric and sulfuric acid. For all samples S*x*N*y* ($x \neq 0$ and $y \neq 0$) the separation occurred leading to clean TRISO particles (see column "TRISO" in Fig. 3) and the acid intercalation into graphene layers seems to swell heterogeneously graphite grains. Graphene layers moved away from each other by groups of hundreds and the solids structure present a lot of cracks. The thickness of the oPyC layer of the TRISO particles was measured by SEM on cross sections (Fig. 4A) at 25 μm, equivalent to a loss of 15 μm during the 15 min microwave treatment. Fig. 5 shows the porous surface of partially oxidized oPyC following MW treatment. The data show that the oPyC layer thickness has diminished due to partial oxidation. It can be concluded that the MW treatment damaged the oPyC, certainly due to the high power applied (1400 W). The TEM view with the dark edges around grains indicates a change in the orientation of the crystal, like a "saucer" (*c*-axis becomes perpendicular to the

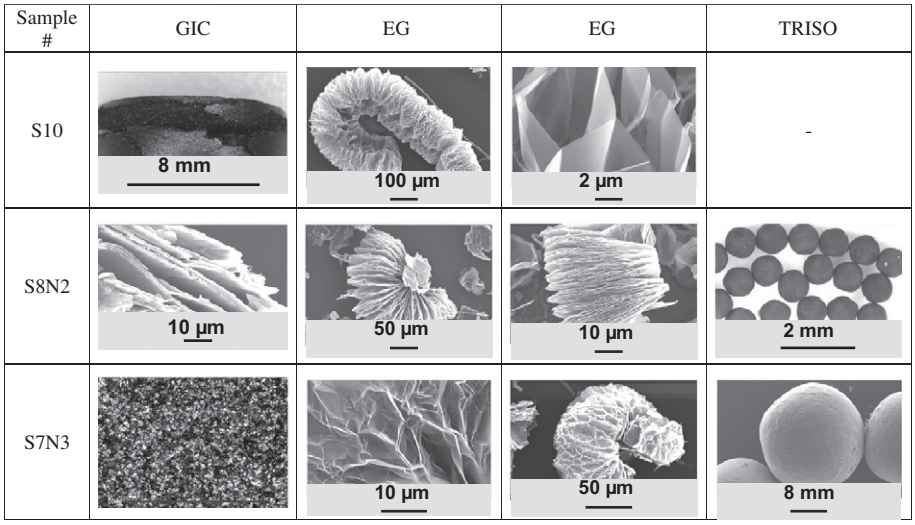

Fig. 3. Optical and SEM pictures of graphite intercalation compounds (GICs), exfoliated graphite (EG) and TRISO particles via MW.

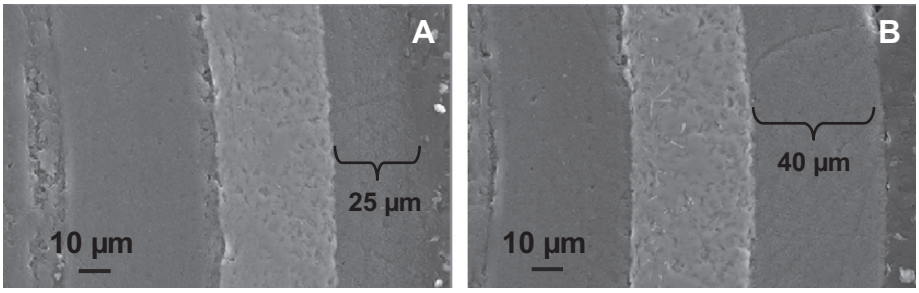

Fig. 4. Representative SEM cross sections of TRISO particles (embedded into a resin) after microwave (MW) treatment (A) and room temperature (RT) treatment (B), showing the oxidation of the outer pyrolytic carbon (oPyC) layer during the MW treatment.

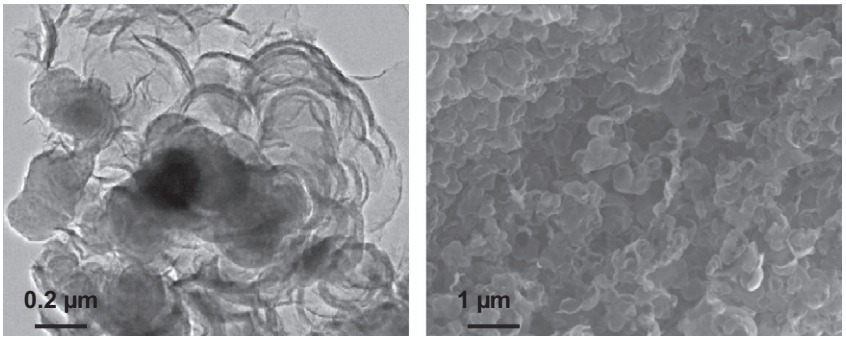

Fig. 5. TEM and SEM photographs of the outer pyrolytic carbon (oPyC) after a microwave (MW) treatment (from S7N3) showing a particle size between 200 and 400 nm.

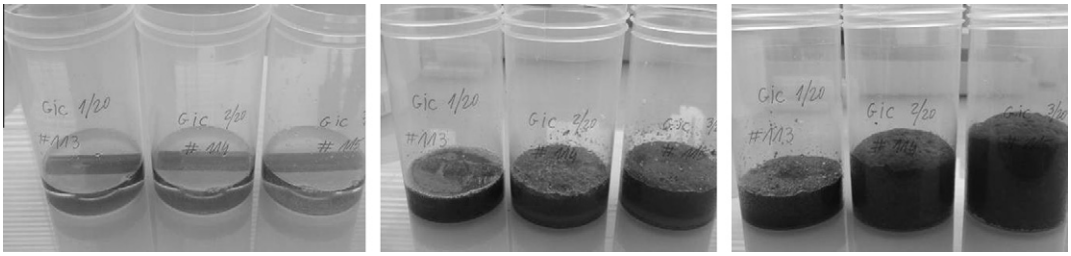

Fig. 6. Samples S20H1, S20H2 and S20H3 at time $t = 0$, $t = 9$ and $t = 17$ min after mixture of H_2SO_4 into H_2O_2.

electron beam). Electronic diffractions on cluster and single crystal revealed both the graphite structure.

3.2. RT treatments

Room temperature treatments on entire compacts showed very strong swelling, as visible in Fig. 6, after a few minutes. Moreover, TRISO particles coatings remain undamaged, as shown in Fig. 4B, the oPyC layer is not oxidized. The volume expansion noted in Table 2 corresponds to the volume of slurry contained in the plastic flasks photographed in Fig. 6, compared to the initial volume of compacts (~5.8 cm^3). The S20H4 sample using 20 mL of H_2SO_4 and 4 mL of H_2O_2 swelled much more after only a few minutes of treatment in comparison to the rest of samples. Gas formation according to the reaction described in (3) contributed to volume expansion. The volume expansion of bulk graphite from the intercalation stage is expected to be higher for high stage (n small) and *vice versa*. We observe the inverse phenomenon due to the decomposition of excessive hydrogen peroxide in the mixture, accelerated by the heat dissipation from the exothermic intercalation reaction. Therefore, the O_2 formation increases the swelling of compacts and favors the separation of TRISO particles from the graphite matrix. For the separation of TRISO particles from the graphite matrix, with this method we do not need the formation of high stage GIC. Nevertheless, high stages could be useful for further treatment (exfoliation) for recycling applications.

In Fig. 7 are presented the four diffractograms of samples S20 Hz ($z = 1$–4). Except for sample S20H2, they present pure phases of H_2SO_4-GIC, without any trace of graphite (no peak at 26.5°). High stage intercalation of pure phases H_2SO_4-GICs obtained via chemical treatments are rarely described in literature (in [6] mixture of stages 3 and 4 are obtained). Thus, the chemical treatment used in this work may be used to prepare high stage intercalation products. Sample S20H2 is partially stage2-H_2SO_4-GIC (peak 0 0 3 is visible at 24°). Results of XRD analyses are given in Table 3 where parameters I_c and d_s are calculated using Eq. (5). For each diffractogram, only the peak with the highest intensity (the peak 0 0 $n + 1$) is used for the calculation of I_c and d_s. I_c shows a highly linear correlation with the stage, that the extrapolation to stage 1 gives $I_c = d_s = 7.773$ Å. d_s seems to increase with high intercalation, maybe due to electronic repulsion between two oxidized graphene layers. This value of 7.77 Å is much lower than those of Lope-Gonzalez et al. [37] (7.98–8.01 Å) but larger than those of Kang et al. [6] (7.62–7.70 Å).

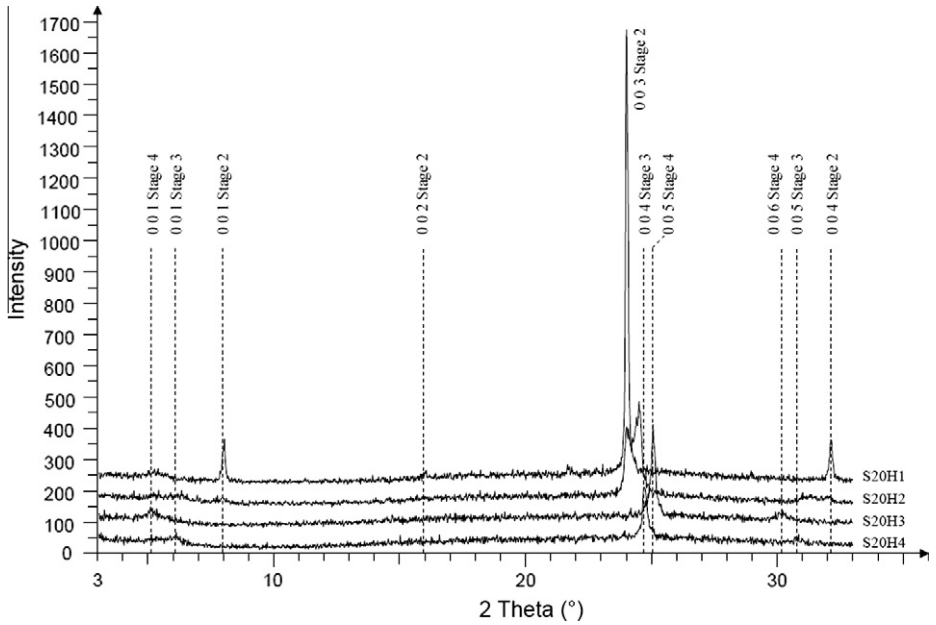

Fig. 7. X-ray diffractograms of H_2SO_4-graphite intercalation compounds (GICs) prepared in mixtures of H_2O_2/H_2SO_4 at room temperature (RT), showing different stages depending on this volume ratio. Step: 0.02°, Step time: 2 s.

Table 3
Diffraction data of stage-2,3,4-H_2SO_4-graphite intercalation compounds (GICs) from diffractograms in Fig. 7.

# Sample	2θ angle (°)	d observed (Å)	Miller index l	Intensity	Stage n	$I_c = d \times l$ (Å)	d_s (Å)
S20H1	7.974	11.0793	1	153	2	11.079	7.747
	15.980	5.5417	2	49		11.083	
	24.021	3.7018	3	1465		**11.105**	
	32.156	2.7814	4	150		11.126	
S20H3	5.074	17.4030	1	76	4	17.403	7.673
	25.066	3.5497	5	340		**17.749**	
	30.233	2.9538	6	62		17.723	
S20H4	6.067	14.5565	1	64	3	14.557	7.676
	24.722	3.5983	4	209		**14.393**	
	30.784	2.9022	5	48		14.511	

Numbers in bold are used to calculate d_s.

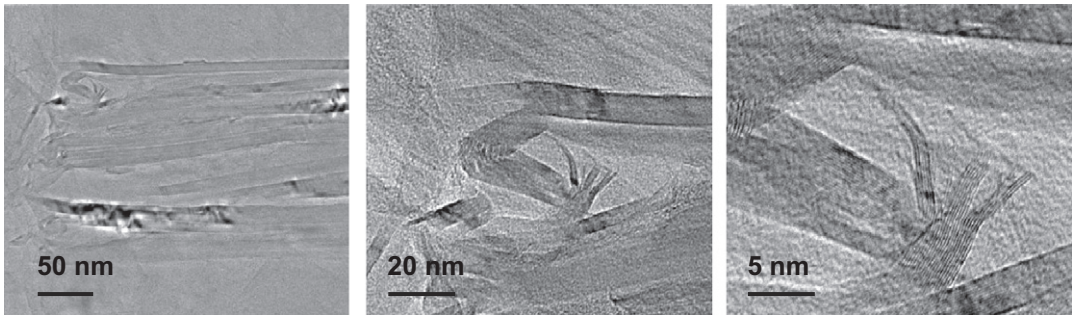

Fig. 8. TEM photographs of exfoliated graphite (EG) from S20H1 showing the graphene layers separation at different scales.

The BET results (Table 2), are in concordance with common data for EG with a regular decrease of specific surface area when n increases (36). The highest value (36.2 m^2/g) represents only 1.33% of the surface area of hypothetic fully exfoliated graphite (~2700 m^2/g, [27,38]). Partly separated graphene layer are shown in Fig. 3 (EG from S10, right) and in Fig. 8. The degree of exfoliation of 1.33% corresponds on average to the separation every 75 graphene plans, which represents a thickness of about 250 Å. This value is very near the L_c (crystallite size) of raw material, suggesting that exfoliation is facilitated where defects into crystals occur in the interface of two crystallites. Fig. 8 shows graphite crystallites with thickness between 100 and 200 Å, and also on the right image graphene sheets by groups of 3, 3, 7, 2 and 5 from right to left. The exfoliation is therefore very

heterogeneous with large undamaged zones and locally highly damaged areas.

An analysis by TEM of GIC was not possible because of its degradation under the electron beam, even at low temperature (−174 °C).

Once compacts are disintegrated, the final separation of TRISO particles from the GIC can be made. The exfoliation process at 1000 °C does not cause the damage of the TRISO coating for all experiments done (with unirradiated materials). Then, particles and exfoliated graphite can be separated from each other using a dense liquid mixture containing bromoforme ($d = 2.89$ g cm^{-3}) and ethanol ($d = 0.79$ g cm^{-3}) at ratio 85%/15% ($d = 2.58$ g cm^{-3}) using a sep funnel. All particles sink in this liquid whereas graphite floats. After washing in ethanol, particles can be treated a few seconds or minutes with ultrasounds to remove graphite traces on their surfaces. In addition, the ultrasound method is another way to disintegrate compacts but its main problem is perhaps the cost due to the enormous energy needed to reach this goal and complex phenomena induced by the sonolyse in water, as mentioned by Guittonneau et al. [39]. Several methods of separation are also proposed and compared in reference [40].

Finally, the intercalation/exfoliation method for this application can be coupled with the method of decontamination of nuclear graphite described by Fachinger et al. [41] in case of irradiated material to remove large proportions of ^{14}C and tritium.

4. Conclusions and perspectives

The present work shows that:

- Clean separation of TRISO particles from the graphite matrix of compacts is possible at room temperature via acid treatment with a mixture of sulfuric acid and hydrogen peroxide. This treatment prevents damaging of the particles, which constitutes the condition *sine qua non* for the success of the separation method applied to the spent TRISO fuel particles. Also, we believe that the developed treatment method could successfully be applied on fuel compacts.
- Industrial recycling of the separated graphite via preparation of the graphite intercalated compounds (GICs) may be an attractive way to recycle this waste for industrial and environmental applications considering the high quality of the GICs and exfoliated graphite (EG) obtained at room temperature.
- However, more research is necessary to better determine the role of amorphous carbon resulting from the phenolic resin and to test the method with irradiated compacts to study the effects of irradiation on the treatment process and on the behavior of the volatile elements such as ^{36}Cl and ^{14}C.

Acknowledgements

The authors would like to thank two microscopists from IMN, Nantes: Éric Gautron for his precious help during TEM analyses and Alain Barreau for his settings of high quality for SEM observations. Specific surface area analyses would not have been possible without the explanations of Éric Chevrel from École des Mines de Nantes. We also like to thank AREVA NC for financial support and AREVA NP for the supply of fuel compacts.

References

[1] IAEA, Characterization, treatment and conditioning of radioactive graphite from decommissioning of nuclear reactors, IAEA-TECDOC-1521, 2006-09.
[2] M. Masson, S. Grandjean, J. Lacquement, S. Bourg, J.M. Delauzun, J. Lacombe, Nucl. Eng. Des. 236 (5–6) (2006) 516–525.
[3] F. Guittonneau, A. Abdelouas, B. Grambow, M. Dialinas, F. Cellier, New methods for HTR Fuel Waste Management, in: Proceedings of the 4th International Topical Meeting on High Temperature Reactor Technology, HTR 2008; 28th September–1st October 2008, ASME, 2008.
[4] A. Abdelouas, S. Noirault, B. Grambow, J. Nucl. Mater. 358 (2006) 1–9.
[5] T. Enoki, M. Suzuki, M. Endo, Graphite Intercalation Compounds and Applications, Oxford University Press, New York, 2003.
[6] F. Kang, Y. Leng, T. Zhang, J. Phys. Chem. Solids 57 (6–8) (1996) 889–892.
[7] F. Kang, Y. Zheng, H. Wang, Y. Nishi, M. Inagaki, Carbon 40 (9) (2002) 1575–1581.
[8] J.H. Han, K.W. Cho, Lee. K-, H. Kim, Carbon 36 (12) (1998) 1801–1810.
[9] B. Tryba, A.W. Morawski, R.J. Kalenczuk, M. Inagaki, Spill Sci. Technol. Bull. 8 (5–6) (2003) 569–571.
[10] B. Tryba, J. Przepiórski, A.W. Morawski, Carbon 41 (10) (2003) 2013–2016.
[11] B. Tryba, A.W. Morawski, K. Kalucki, J. Phys. Chem. Solids 65 (2–3) (2004) 165–169.
[12] B. Tryba, A.W. Morawski, M. Inagaki, Carbon 43 (11) (2005) 2417–2419.
[13] Z. Ying, X. Lin, Y. Qi, J. Luo, Mater. Res. Bull. 43 (10) (2008) 2677–2686.
[14] E.H.L. Falcao, R.G. Blair, J.J. Mack, L.M. Viculis, C. Kwon, M. Bendikov, et al., Carbon 45 (6) (2007) 1367–1369.
[15] J. Li, M. Li, J. Li, H. Sun, Ultrason. Sonochem. 14 (1) (2007) 62–66.
[16] J. Li, Q. Liu, H. Da, Mater. Lett. 61 (8–9) (2007) 1832–1834.
[17] J. Li, J. Li, M. Li, Mater. Lett. 62 (14) (2008) 2047–2049.
[18] M. Inagaki, R. Tashiro, Y. Washino, M. Toyoda, J. Phys. Chem. Solids 65 (2–3) (2004) 133–137.
[19] D.D.L. Chung, J. Mater. Sci. 22 (1987) 4190–4198.
[20] M. Toyoda, K. Moriya, J. Aizawa, H. Konno, M. Inagaki, Desalination 128 (3) (2000) 205–211.
[21] M. Inagaki, H. Konno, M. Toyoda, K. Moriya, T. Kihara, Desalination 128 (3) (2000) 213–218.
[22] M. Inagaki, K. Shibata, S. Setou, M. Toyoda, J. Aizawa, Desalination 128 (3) (2000) 219–222.
[23] M. Toyoda, Y. Nishi, N. Iwashita, M. Inagaki, Desalination 151 (2) (2003) 139–144.
[24] M. Toyoda, J. Aizawa, M. Inagaki, Desalination 115 (2) (1998) 199–201.
[25] M. Toyoda, M. Inagaki, Carbon 38 (2) (2000) 199–210.
[26] M. Toyoda, M. Inagaki, Spill Sci. Technol. Bull. 8 (5–6) (2003) 467–474.
[27] A. Celzard, J.F. Marêché, G. Furdin, Prog. Mater. Sci. 50 (1) (2005) 93–179.
[28] M.P. Vitali, Processes and major equipment for the production of compacts HTR fuel. Eurocourse 2 in Petten, Netherlands, 4–7 December, 2007.
[29] F. Charollais, M.P. Vitali, C. Perrais, M. Perez, D. Moulinier, Latest achievements of CEA & AREVA NP on HTR fuel fabrication, in: Proceedings of HTR 2006, Johannesburg, South Africa, October 1–4, 2006.
[30] A. Müller, Establishment of the technology to manufacture uranium dioxide kernels for PBMR fuel, in: Proc. HTR 2006, Johannesburg, South Africa, October 1–4, 2006.
[31] D.A. Petti, J. Buongiorno, J.T. Maki, R.R. Hobbins, G.K. Miller, Nucl. Eng. Des. 222 (2003) 281–297.
[32] P. Bros, M.H. Mouliney, D. Millington, A. Sneyers, J. Fachinger, K. Vervondern, et al., Raphaël project – HTR specific waste characterization programme, in: Proc. HTR 2006, Johannesburg, South Africa, October 1–4, 2006.
[33] IAEA, Evaluation of high temperature gas cooled reactor performance: benchmark analysis related to initial testing of the HTTR and HTR-10, IAEA-TECDOC-1382, 2003.
[34] M.A. Fütterer, G. Berg, A. Marmier, E.H. Toscano, K. Bakker, Irradiation results of AVR fuel pebbles at increased temperature and burn-up un the HFR Petten, in: Proc. HTR 2006, Johannesburg, South Africa, October 1–4, 2006.
[35] Handbook of Chemistry and Physics, CRC Press, 2004.
[36] G. Furdin, Fuel 77 (6) (1998) 479–485.
[37] J.D. Lopez-Gonzalez, A.M. Rodriguez, F.D. Vega, Carbon 7 (1969) 583–588.
[38] A. Celzard, J.F. Marêché, G. Furdin, Carbon 40 (14) (2002) 2713–2718.
[39] F. Guittonneau, A. Abdelouas, B. Grambow, S. Huclier, Ultrasonic Sonochemistry 17 (2010) 391–398.
[40] F. Guittonneau, Développement de stratégies de gestion du combustible HTR. PhD Thesis, Université de Nantes, Nantes, 2009.
[41] J. Fachinger, W. von Lensa, T. Podruhzina, Nucl. Eng. Des. 238 (2008) 3086–3091.